ELECTROCHEMICAL ENERGY STORAGE BEHAVIOR OF Sn/SnO_2 AND Sn/SnO_2/MWCNT NANOCOMPOSITE ANODES FOR Li-ION BATTERIES

H. Akbulut* and M. Alaf

Sakarya University, Engineering Faculty, Dept. of Metallurgy and Materials Engineering, Esentepe Campus, 54187, Sakarya, TURKEY
**akbulut@sakarya.edu.tr*

Keywords: tin oxide, nanocomposite, energy storage, discharge capacity, Li-ion batteries.

Abstract

In this study, tin/tinoxide (Sn/SnO_2) films and tin/tinoxide/multi walled carbon nano tube (Sn/SnO_2/MWCNT) composites were produced by thermal evaporation and subsequent plasma oxidation as anode materials for Li-ion batteries. Sn/SnO_2 coated on stainless steel substrates and Sn/SnO_2 coated on MWCNT buckypapers were used as working electrodes in assembled as coin-type (CR2016) test cells. The ratio between metallic tin (Sn) and tinoxide (SnO_2) was controlled with plasma oxidation time and effects of the ratio were investigated on the structural and electrochemical properties.

1 Introduction

Lithium-ion batteries (LIBs) offer significant advantages in weight and energy density over other rechargeable batteries. They have proven to be ideal for small-scale portable electronic applications such as cellular phones and laptop computers. Emerging applications in implantable medical devices also take advantage of the high cycle life, light weight and other benefits of LIBs [1-2]. Among LIBs anode materials, SnO_2-based materials have become one of the promising candidates, as SnO_2 has high theoretical capacity, the environmental friendliness of its raw material processing and low cost. In theory, SnO_2 exhibit a first discharge capacity of 1494 mAh g^{-1} and a reversible discharge capacity of 782 mAh g^{-1}[3]. However, the practical application of SnO_2-based materials has been restrained by their cycling performance, resulting from a large-volume change during the charge and discharge processes. This excessive volume change leads to electrode pulverization and electrical disconnection [4]. To overcome this problem, there have been many studies of combining Sn-based material with other materials to form composite electrodes with the intention to increase the dispersion of Sn-based oxide in other oxide matrix and/or surface. Using of Sn/SnO_2 composites could be a solution in realizing increased reversible capacity as well as reduced irreversible capacity and capacity fade upon cycling, as this could increase the $Sn:Li_2O$ ratio in the anode matrix[5]. Other effective strategies to alleviate this problem is to disperse tin based materials in a carbon matrix or encapsulate them with carbon to accommodate the strain of volume change during the alloying and dealloying processes of Li–Sn. Among them, the SnO_2/carbon nanotube (CNT) composites have attracted considerable research effort [6]. CNTs, because of their unique 1D tubular structure, high electrical and thermal conductivities and extremely large surface area, have been considered as ideal additive materials to improve

the electrochemical characteristics of the electrode of LIBs. CNT based electrode materials have been recently studied by many research groups [7]. However, limited research work has been done on the fabrication and evaluation of a "free-standing" CNT paper electrode without any electrode substrate that is produced with a simple filtration method [8]. CNT paper, also called buckypapers, are self-supporting networks of entangled CNT assemblies arranged in a random fashion and held together by van der Waals interactions at the tube–tube junctions [9].

In our present work, Sn/SnO_2 films and Sn/SnO_2/MWCNT) composites were produced by thermal evaporation and plasma oxidation as anode materials for Li-ion batteries. Sn/SnO_2 coated on stainless steel substrates and Sn/SnO_2 coated on MWCNT buckypapers were used as working electrode in coin-type (CR2016) test cells. The ratio between metallic tin (Sn) and tinoxide (SnO_2) was controlled with plasma oxidation time and effects of the ratio were investigated on the morphological and electrochemical properties.

2. Experiment Details

2.1 Functionalization of MWCNT and preparing of buckypapers

MWCNTs over 1.0 μm in length with the outer diameter of 50 nm were purchased from Arry Nano (Germany). Since the mechanical properties of buckypapers are primarily determined by the tube–tube interactions, chemical functionalization of the MWCNT sidewalls and tips could be utilized to increase the modulus and strength of the MWCNT buckypapers. Chemical oxidation of MWCNTs was carried out with a mixture of H_2SO_4 and HNO_3 acids in ratio 3:1 for 3 h after annealing and treating in HCl acid for impurity removing. The functionalized MWCNTs were first dispersed into water by the aid of SDS surfactant and sonicated to form a well-dispersed suspension which subsequently was vacuum filtered through PVDF membrane filters of 220 nm pore size to form buckypapers. In each experiment, a MWCNT suspension at a concentration of 1mg/ml was prepared by tip sonication for 60 min. Then the resulting solid was washed up and the sample dried in the vacuum at 40°C for overnight and the MWCNT films were peeled-off from the membrane.

2.2 Production of Sn films and Sn/MWCNT composites via thermal evaporation

Thermal evaporation of metallic tin on the stainless steel substrates and buckypapers was performed in a multifunctional PVD unit. High purity metallic tin (99.999%) was placed in a Mo boat in the deposition chamber, which was evacuated to 10^{-4} Pa and then backfilled with argon to a pressure of 1 Pa to produce Sn films and Sn/MWCNT composites.

2.3 Production Sn/SnO_2 and Sn/SnO_2/MWCNT composites via RF plasma oxidation

Sn/SnO_2 and Sn/SnO_2/MWCNT composites were produced by RF plasma oxidation from the thermally evaporated pure Sn films and Sn/MWCNT composites, respectively. Plasma oxidation of the Sn films was conducted using high-purity oxygen (99.999%) and argon (99.9999%) gas mixture in ratio 1:1. Three different oxidation times of 30, 45 and 60 min. were chosen. Total chamber pressure and RF power for each oxidation were kept constant at 1.6 Pa, and 80 W. Fig. 1 represents the methods of preparing Sn based anode materials.

2.4. Characterization of nanocomposites

An X-ray diffractometer (XRD-Rigaku D/MAX 2000) with Cu-Kα radiation has been used to determine the composition, relative phase amounts and structure of the composites. FE-SEM (JEOL 6335F), SEM (JEOL 6060LV) and AFM (Quesant) were used for examine surface morphologies. Coin-type (CR2016) test cells were assembled in an argon-filled glove box, directly using the Sn/SnO_2 coated stainless steel substrates and Sn/SnO_2/MWCNT composite

free-standing electrodes as working electrodes, a lithium metal foil as the counter electrode, a micro porous polypropylene (PP) membrane (Cellgard 2300) as the separator, and 1M solution of $LiPF_6$ in ethylene carbonate (EC) and dimethyl carbonate (DMC) (1:1 by weight) as the electrolyte. The cells were cyclically tested on a MTI BST8-MA Battery Analyzer using different current density over a voltage range of 0.1–2V and 0.5–3V and EIS measurements using Gamry Instrument Version 5.67for Sn/SnO_2 and Sn/SnO_2/MWCNT.

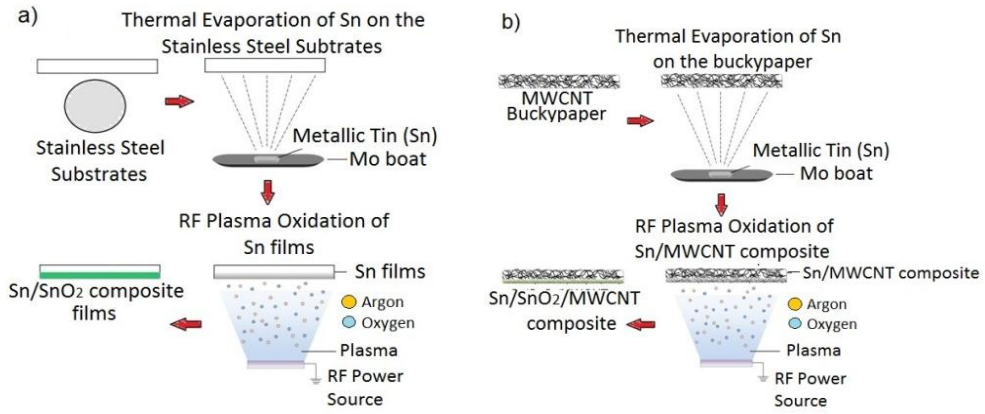

Figure 1. Schematic representations of methods for preparing a) Sn/SnO_2 and (b) Sn/SnO_2/MWCNT composites

3. Results and Discussion

3.1 Characteristics of Buckypapers

The buckypapers were successfully produced as flexible, uniform, smooth and crack-free disks and easily peeled-off from PVDF membrane. FESEM surface image and cross-section of the buckypapers electrodes are shown in Fig. 2. The inset of Fig. 2a shows a photograph of the MWCNT paper held by tweezers, indicating the good flexibility. Porous structure that appropriate for composite manufacturing was obtained as shown in Fig. 2b. Cross-section area of the buckypaper is homogenous and approximate thickness is 80 μm (Fig. 2c).

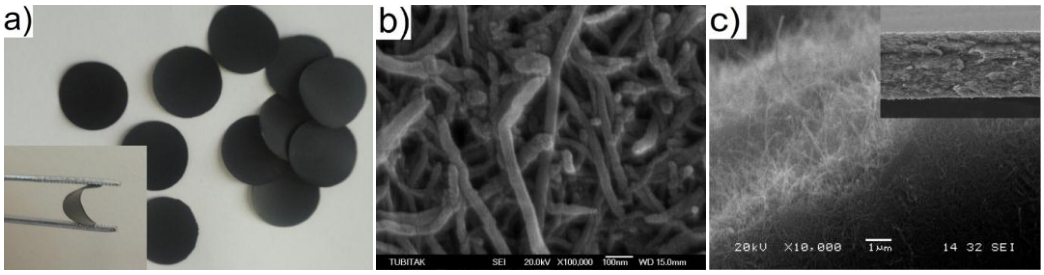

Figure 2. a) Flexible free-standing MWCNT buckypapers, b) FESEM image of buckypaper and c) cross-section.

3.2. Characteristics of Sn films and Sn/MWCNT nanocomposites

Fig. 3 shows a typical XRD pattern for the pure tin (Sn) film evaporated onto the stainless steel substrates (JCPDS file no: 01-089-2958 for powder Sn) and a SEM image. The (220), (211) and (200) peaks are the strongest. After thermal evaporation onto a stainless steel substrate, tin exhibits a crystalline microstructure with epitaxial grains as shown in Fig. 3b. The grain sizes calculated with Scherer's formula and found 34 nm. In order to produce Sn/MWCNT composites, pure metallic tin (Sn) was thermally evaporated on the buckypapers having controlled porosity. Fig. 4a presents the XRD patterns of Sn/MWCNT composite could be indexed as tin and carbon, with all peaks corresponding well to standard crystallographic data (Sn:JCPDS No. 01-089-2958 C:JCPDS No. 00-026-1080). No other impurities were detected, which indicates the high-purity products. SEM images of Sn/MWCNT composites are shown in Fig. 4b, which exhibits thermally evaporated Sn on the

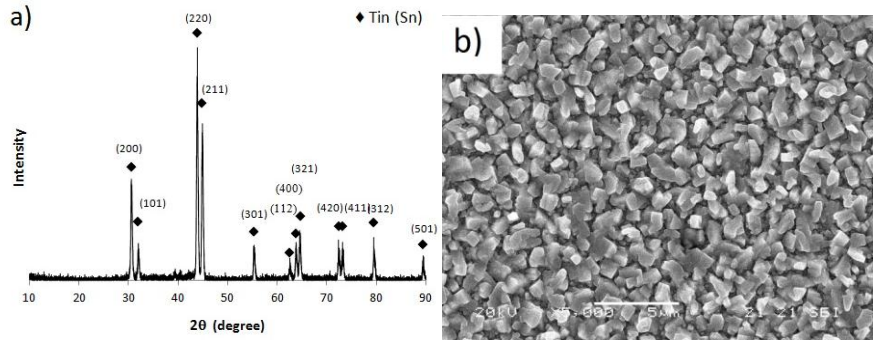

Figure 3. a) XRD pattern and b) SEM image of pure tin (Sn) film evaporated at 1 Pa Ar pressure.

surfaces of MWCNTs forming a core-shell structure. Evaporated tin deposited not only buckypapers but also penetrated into porous MWCNTs network. Shafiei et al. [10] produced a thin-film Sn deposited on the carbon fiber paper (CFP) composite electrode by electrodeposition and showed the SEM images similar to our surface morphology results.

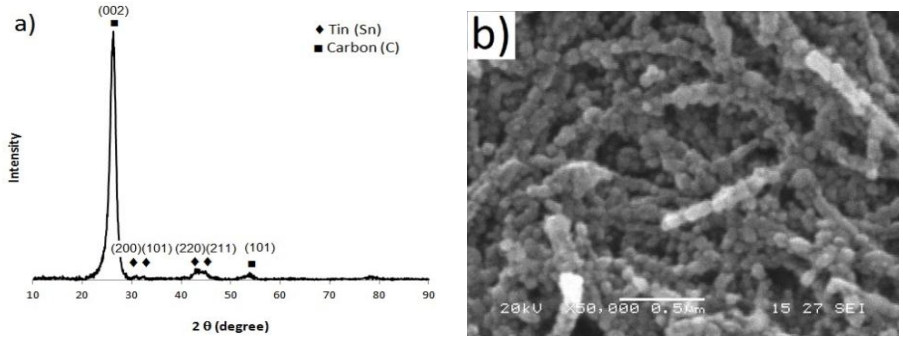

Figure 4. a) XRD pattern of Sn/MWCNT composite and b) SEM image of Sn/MWCNT nanocomposites.

Fig. 5 shows SEM-EDX dot-map analysis for Sn/MWCNT composite. Sn rich layer depth is about 5 μm and evaporated tin is mainly introduced between the MWCNTs filling the pores. It can be concluded from the dot-map analysis that Sn shows a gradient composition through the center of buckypaper. It is well known the gradient phase distribution in the composites is beneficial for decreasing crack initiation and therefore, failure [11].

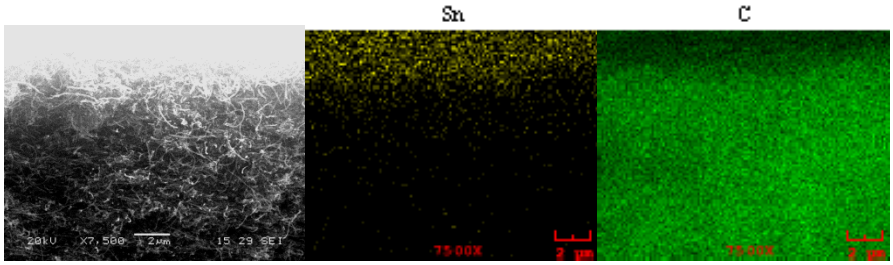

Fig. 5. SEM-EDX dot-map analysis results for Sn/MWCNT nanocomposite

3.3. Characteristics of Sn/SnO_2 and Sn/SnO_2/MWCNT nanocomposites

After the thermal evaporation process, the Sn and Sn/MWCNT samples were subjected to a RF plasma oxidation process for three different oxidation times of 30, 45 and 60 min. to produce Sn/SnO_2 and Sn/SnO_2/MWCNT nanocomposites. Information about the composition and crystallinity was obtained using XRD, which is presented in Fig. 6a. The films have a Sn and SnO_2 structure, which agrees well with the standard data files (Sn:JCPDS No. 01-089-2958 and SnO_2: JPDS No. 00-041-1445), and all of the films have a crystalline structure.

Increasing oxidation time resulted in increasing intensity of SnO_2 peak while decreasing of Sn peak. The SEM morphology of Sn/SnO_2 films produced at various plasma oxidation times including 45 and 60 min. are presented in Fig. 6b, 6c and shows very fine SnO_2 nanoparticles with increasing oxidation time. Sn/MWCNT composites were subjected to plasma oxidation to produce Sn/SnO_2/MWCNT nanocomposites. Characterization of Sn/SnO_2/MWCNT composites was investigated through XRD and the results are shown in Fig. 7. Fig. 7a shows the diffraction peaks at 26°and 33° correspond to SnO_2 (JCPDS No. 00-041-1445) while the peak at 45°for Sn (JCPDS No.01-089-2958). Increasing oxidation time resulted in increasing intensity of SnO_2 peak. It should be noted that a diffraction peak at around 26°, which is the main peak of tetragonal SnO_2 (110) almost overlaps with the main peaks of hexagonal C (002) as also defined in the different works [12]. FWHM values of the main peaks for samples were calculated and are shown in Fig. 7b. Comparing all spectra and FWHM values, it is easy to find that broadening peaks is mainly contributing from increasing SnO_2 amount.

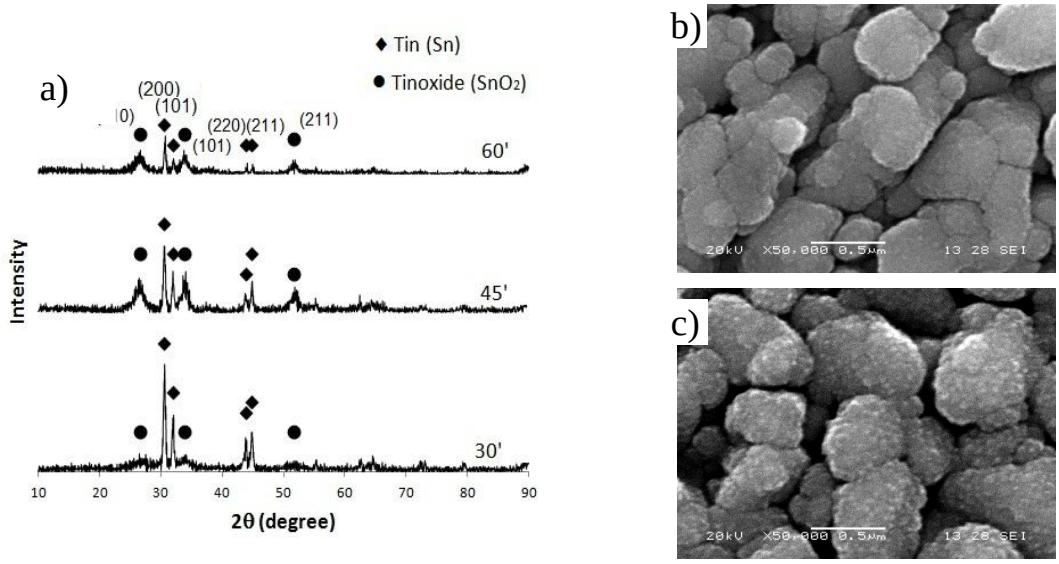

Figure 6. a) XRD patterns of the (Sn/SnO_2) composite films b) SEM images Sn/SnO_2 composite films produced by plasma oxidation for 45 min. and c) 60 min.

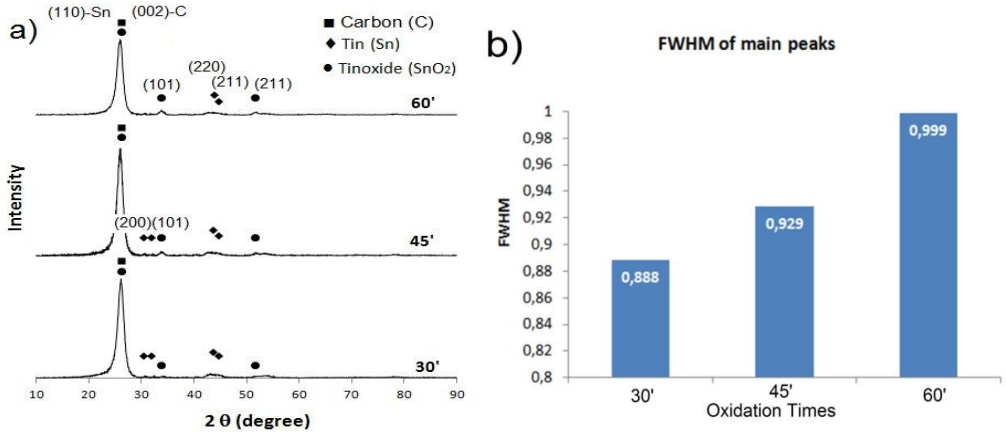

Figure 7. a) XRD patterns of Sn/SnO_2 composite films produced by plasma oxidation for 30, 45 and 60 minutes and b) FWHM values of the main peaks.

Fig. 8. presents FESEM images of Sn/SnO_2/MWCNT composites shows the effect of three different oxidation time. As seen, Sn based phases were deposited around the MWCNTs forming a core-shell structure. Gao et al. [13] presented CNTs coated with thick layers of

SnO_2 TEM images similar to our results. Since surface functionalization of MWCNTs creates defects on the sp^2 bonds, it is an expected phenomenon of nucleation and growth of SnO_2 on the MWCNT phase. As can be seen from the high magnification micrographs located at the upper-right corner of the Fig. 8, SnO_2 is deposited on the MWCNT surfaces showing core-shell structure. Increasing oxidation time resulted in thicker SnO_2 based phase on the MWCNT surfaces. Sn/SnO_2/MWCNT composite produced by oxidation for 60 min. on MWCNT was examined with AFM and shown in Fig. 9 (lateral sizes of 10 µm×10 µm and 1µm×1 µm). For all composites, quantitative phase analysis was performed in order to determine the relative phase amounts using Reitveld refinement method, as shown in Fig. 10. Increasing oxidation time resulted in increasing tin oxide percent and decreasing Sn percent.

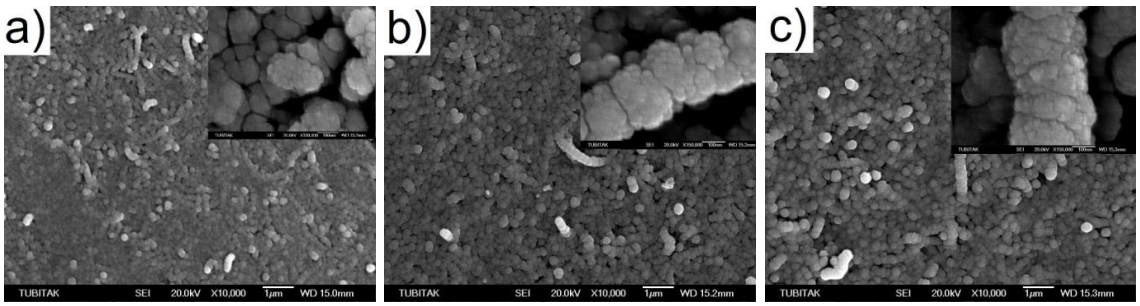

Figure 8. FESEM images Sn/SnO_2/MWCNT composites produced by plasma oxidation for a) 30 min., b) 45 min. and c) 60 min. after thermal evaporation of Sn onto MWCNT buckypapers

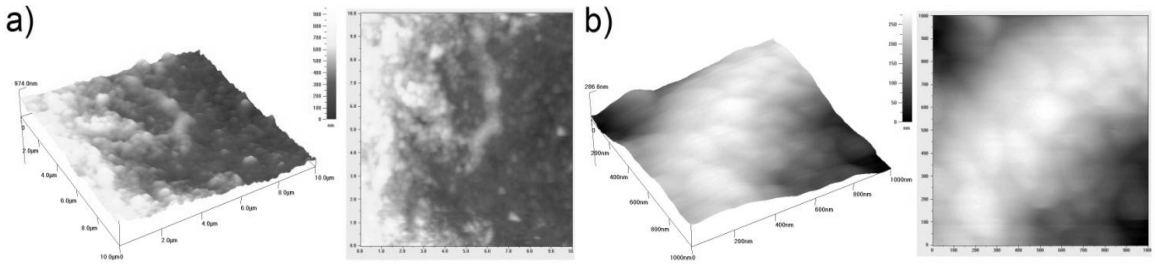

Figure 9. 3D and top views AFM images of Sn/SnO_2/MWCNT composite (a) 10µm×10 µm (b)1µm×1 µm.

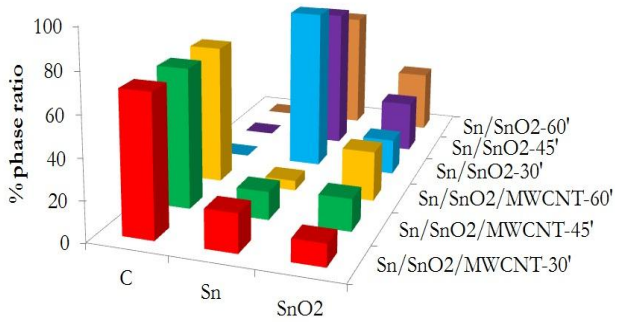

	C	Sn	SnO2
Sn/SnO2/MWCNT-30'	70	19	11
Sn/SnO2/MWCNT-45'	70	14	16
Sn/SnO2/MWCNT-60'	70	5	25
Sn/SnO2-30'	0	82	18
Sn/SnO2-45'	0	73	26
Sn/SnO2-60'	0	62	32

Figure 10. Percent of phase ratio of Sn/SnO_2 and Sn/SnO_2/MWCNT composites

3.4. Electrochemical Results

The discharge capacity vs. the number of cycles for cells made from Sn/SnO_2 films is shown in Fig. 11a. The results show that the specific discharge capacities of the Sn/SnO_2 films increases with increasing amount of SnO_2 in the composites. Similar relationship between SnO_2 ratio and specific capacity values have been obtained by Sivashanmugam et al. [3]. Although, relatively high discharge capacities were obtained in the Sn/SnO_2 double phase electrodes, very low capacity retention is seen to be the obstacle for these electrodes. The cells

assembled from Sn/SnO_2 on the stainless steel were failed after approximate 20 cycles. It is believed because of Sn based electrode disintegration caused by a high-volume increase [6].

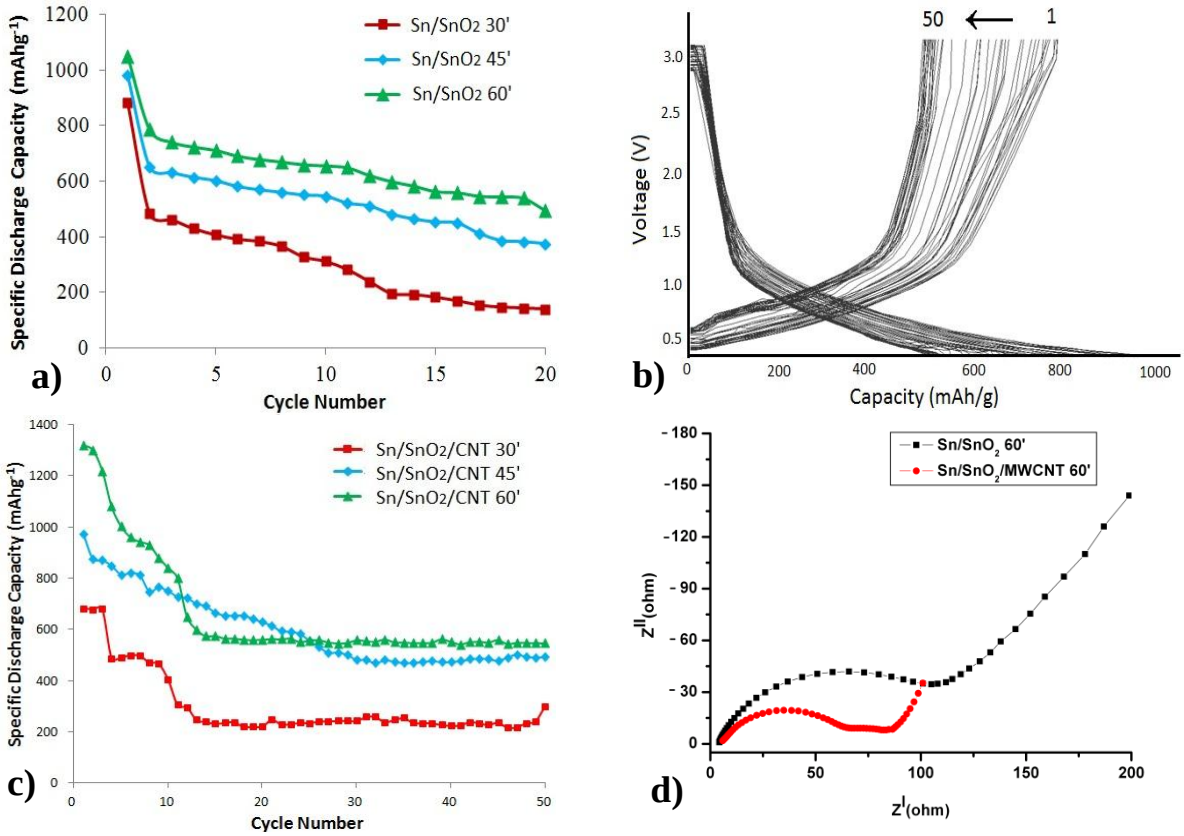

Figure 11. a) Specific discharge capacities of Sn/SnO_2 composite films b) Charge-discharge voltage profiles of Sn/SnO_2/MWCNT 45' for 50 cycles c) specific discharge capacities of Sn/SnO_2/MWCNT composite electrodes d)Electrochemical impedance spectra of Sn/SnO_2 and Sn/SnO_2/MWCNT 60' oxidation

Nanocomposites electrodes of Sn/SnO_2/MWCNTs showed better performances. Even at 50 cycles no cell failure was detected all the studied cell assemblies. As an example the charge-discharge curve is presented for the nanocomposite oxidized for 45 min. As can be seen from Fig. 11b, a very low amount of capacity fade is obtained after 50 cycles. Fig. 11c displays cycling stability of the Sn/SnO_2/MWCNT composite electrodes at the voltage range between 0.5–3V. The capacity retention for the first 10 cycles is maintained as 63%, 76% and 60% for the Sn/SnO_2/MWCNT composites electrodes plasma oxidized for 30, 45 and 60 min., respectively. At 50 cycles, the discharge capacities are still 298, 493, 546 $mAhg^{-1}$ and capacity retentions after 50 cycles are 43%, 50% and 41% for the Sn/SnO_2/MWCNT composites electrodes, oxidized for 30, 45 and 60 min., respectively. At the cycle number of 15 Sn/SnO_2/MWCNT nanocomposite oxidized for 60 min. showed very sharp capacity decrease but remained nearly constant up to 50 cycles and exhibited a discharge capacity of 546 $mAhg^{-1}$. Electrochemical impedance measurements were carried out and, for brevity, only two measurements are presented in Fig 11d and shows interphase electronic contact resistance decreases by using MWCNT buckypapers in the Sn/SnO_2 active materials. This shows Sn/SnO_2/MWCNT nanocomposite electronic conductivity of the anode was improved.

4. Conclusions

Nanocrystalline Sn/SnO_2 composite thin films were successfully produced by coating on stainless steel substrates and MWCNT buckypapers using two steps: thermal evaporation and R.F. plasma oxidation. Increasing plasma oxidation time caused to increase SnO_2 ratio in

Sn/SnO_2 films. Microstructural and XRD investigations showed Sn/SnO_2 double phases are coated on the MWCNTs forming a core-shell structure. Discharge capacity measurements showed that forming Sn/SnO_2 on the MWCNTs resulted in not only high discharge capacities, but also high-capacity retention. For instance, Sn/SnO_2 produced on the stainless steel failed almost in 20-25 cycles whereas Sn/SnO_2/MWCNT nanocomposites prevented a discharge capacity of 546 mAh g^{-1} even at 50 cycles. Electrochemical impedance measurements also showed that nanocomposites exhibit low interphase electronic contact resistance in comparison with Sn/SnO_2 formed on stainless steel substrates.

Acknowledgements
This work is supported by the Scientific and Technological Research Council of Turkey (TUBITAK) under the contract number 109M464. The authors thank the TUBITAK MAG workers for their financial support.

References

[1] Krieger E.M., Arnold C.B. Effects of undercharge and internal loss on the rate dependence of battery charge storage efficiency. *J. Power Sources* **210**, pp. 286–291(2012).
[2] Casas C., Li W. A review of application of carbon nanotubes for lithium ion battery anode material. *J. Power Sources* **208**, pp. 74–85 (2012).
[3] Sivashanmugam A., Kumar T.P., Renganathan N.G., Gopukumar S., Wohlfahrt-Mehrens M., Garche J. Electrochemical behavior of Sn/SnO_2 mixtures for use as anode in lithium rechargeable batteries. *J. Power Sources* **144**, pp. 197–203 (2005).
[4] Han S., Jang B., Kim T., Oh S.M., Hyeon T. Simple synthesis of hollow tin dioxide microspheres and their application to lithium-ion battery anodes. *Advanced Functional Materials* **15**, pp. 1845–1850 (2005).
[5] Kim Y., Yoon Y., Shin D., Fabrication of Sn/SnO_2 composite powder for anode of lithium ion battery by aerosol flame deposition. *J. Analytical & Applied Pyrol.* **85** pp. 557–560 (2009).
[6] Fu Y., Ma R., Shu Y., Cao Z., Ma X. Preparation and characterization of SnO_2/carbon nanotube composite for lithium ion battery applications. *Mater. Let.* **63** pp. 1946–1948 (2009).
[7] Ren J., Yang J., Abouimrane A., Wang D., Amine K. SnO_2 nanocrystals deposited on multiwalled carbon nanotubes with superior stability as anode material for Li-ion batteries. *J. Power Sources* **196** pp. 8701– 8705 (2011).
[8] Noerochim L., Wang J.Z., Chou S.L., Wexler D., Liu H.K. Free-standing SWCNT/SnO_2 anode paper for flexible lithium-ion batteries *Carbon* **50** pp. 1289–1297 (2012).
[9] Spitalsky Z., Aggelopoulos C. Tsoukleri G. Tsakiroglou C. Parthenious J. Georga S. Krontiras C. Tasis D. Papagelis K. Galiotis C. The effect of oxidation treatment on the properties of MWCNT thin films. *Mater. Science and Engineer. B* **165** pp. 135–138 (2009).
[10] Shafiei M., Alpas A.T., Electrochemical performance of a tin-coated carbon fibre electrode for rechargeable lithium-ion batteries. *J. Power Sources* **196** pp. 7771–7778 (2011).
[11] Tilbrook M. T., Moon R. J, Hoffman M. Crack propagation in graded composites. *Composites Science and Technology* **65** pp. 201–220 (2005).
[12] Han W., Zettl A. Coating single-walled carbon nanotubes with tin oxide. *Nano Letters* **3** pp. 681–683 (2003).
[13] Zhao L., Gao L. Coating of multi-walled carbon nanotubes with thick layers of tin(IV) oxide. *Carbon* **42** 1858–1861 (2004).